coatings

Article

Effect of Laser Remelting of Fe-Based Thermally Sprayed Coating on AZ91 Magnesium Alloy on Its Structural and Tribological Properties

Martin Buchtík [1,*], Matěj Březina [1], Libor Mrňa [2,3], Marek Palán [4], Jan Filipenský [5], Pavel Doležal [1,3], David Nečas [3], Josef Frýza [3], Daniel Kajánek [6], Jaromír Wasserbauer [1] and Leoš Doskočil [1]

[1] Materials Research Centre, Faculty of Chemistry, Brno University of Technology, Purkynova 464/118, 612 00 Brno, Czech Republic; brezina@fch.vut.cz (M.B.); dolezal@fme.vutbr.cz (P.D.); wasserbauer@fch.vut.cz (J.W.); doskocil@fch.vut.cz (L.D.)
[2] Institute of Scientific Instruments of the Czech Academy of Sciences, Kralovopolska, 147, 612 64 Brno, Czech Republic; mrna@isibrno.cz
[3] Faculty of Mechanical Engineering, Brno University of Technology, Technicka 2896/2, 602 00 Brno, Czech Republic; david.necas@vut.cz (D.N.); fryza@fme.vutbr.cz (J.F.)
[4] Department of Materials and Engineering Metallurgy, Faculty of Mechanical Engineering, University of West Bohemia, Univerzitni 22, 301 00 Plzen, Czech Republic; marek@palan.cz
[5] PLASMAMETAL, Ltd., Tovarni 917/1e, 643 00 Brno, Czech Republic; filipensky@plasmametal.cz
[6] Research Centre, University of Zilina, Univerzitna 8215/1, 010 26 Zilina, Slovakia; daniel.kajanek@uniza.sk
* Correspondence: buchtik@fch.vut.cz; Tel.: +420-541-149-469

Abstract: An Fe-based coating was thermally sprayed onto the surface of AZ91 magnesium alloy via the High-Velocity-Oxygen-Fuel (HVOF) method. The thermally sprayed coating with a thickness of 530 ± 25 µm and a porosity of 0.7 ± 0.1% did not show any macrostructural defects and did not cause any degradation of the AZ91 alloy. Laser remelting of the surface layer of the sprayed coating resulted in the recrystallization of the structure and the disappearance of presented pores, splat boundaries, and other defects. This led to an increase in the hardness of the remelted layer from the original 535 ± 20 HV0.3 up to 625 ± 5 HV0.3. However, during the laser remelting at a laser power of 1000 W, stress cracking in the coating occurred. The tribological properties were evaluated by the ball-on-plate method under dry conditions. Compared to the uncoated AZ91 magnesium alloy, a higher value of friction coefficient (COF) was measured for the as-sprayed coating. However, there was a decrease in wear rate and weight loss. The remelting of the surface layer of the as-sprayed coating led to a further decrease in the wear rate and weight loss. Based on the obtained data, it has been shown that the application of laser-remelted thermally sprayed Fe-based coatings on AZ91 Mg alloy improves hardness and tribological properties compared to bare Mg alloy and as-sprayed Fe-based coatings.

Keywords: AZ91; magnesium alloy; HVOF coating; laser remelting; tribological properties; wear behavior

check for updates

Citation: Buchtík, M.; Březina, M.; Mrňa, L.; Palán, M.; Filipenský, J.; Doležal, P.; Nečas, D.; Frýza, J.; Kajánek, D.; Wasserbauer, J.; et al. Effect of Laser Remelting of Fe-Based Thermally Sprayed Coating on AZ91 Magnesium Alloy on Its Structural and Tribological Properties. *Coatings* **2023**, *13*, 1033. https://doi.org/10.3390/coatings13061033

Academic Editor: Manuel António Peralta Evaristo

Received: 12 May 2023
Revised: 26 May 2023
Accepted: 30 May 2023
Published: 2 June 2023

1. Introduction

Magnesium alloys are used in industry, especially in the automotive industry, the aerospace industry, electrical engineering, and telecommunications, due to their low densities, which are the lowest of any currently known metallic construction materials, and due to their high strength-to-weight ratios [1–4]. Current applications in the automotive industry include their use for components such as pedals, engine block castings, gearbox housings, seat frames, and some bodywork components, etc. [1,5]. In industrial engineering, such as in textiles or printing, magnesium alloys are used for components operating at high speeds and which therefore need to be lightweight to minimize inertial forces [1,5].

However, a common feature of all magnesium alloys is their low resistance to corrosion and wear [1,6–9]. These disadvantages can be avoided by the application of protective coatings [7,9–12]. Many types of coatings have been developed to increase the corrosion resistance of magnesium materials, for example, plasma electrolytic oxidation (PEO) coatings [13], layered double hydroxides (LDH), superhydrophobic coatings [14,15], electroless coatings or electroplated coatings [16–18], phosphate coatings or coatings deposited via hot spray technology [3,19–21]. Although these coatings increase corrosion resistance, they achieve low adhesion, hardness and abrasion resistance, which limits their practical application [22,23].

In addition to the above-mentioned applications of protective coatings, the addition of alloying elements or the use of heat or mechanical treatment (e.g., shot peening [24–26], laser shot peening [27], laser cladding [28] or friction stir welding [29] are also used to improve the surface properties of Mg alloys.

As reported in publications [30–33], the addition of an alloying element such as Nd, Sc or Sm to AZ91 alloy resulted in improved corrosion properties and increased hardness, reduced wear rate and increased strength. A suitable alternative could also be the application of coatings by mechanical alloying followed by laser cladding technique [28]. The application of FeCoNiCrAl/AlSi12-based composite coatings by the mechanical alloying method can increase the hardness and nanohardness of the sample surface. Subsequent laser cladding of the FeCoNiCrAl/AlSi12 coating resulted in a further significant increase in hardness. The coating exhibited a refined and homogeneous microstructure without structural defects such as pores and cracks.

In recent years, the most promising methods for the preparation of coatings appear to be the High-Velocity-Oxygen-Fuel (HVOF) and Cold Spray (CS) methods [20,22,34]. Both HVOF and CS are thermal spraying techniques, allowing the deposition of dense, hard, and low porous coatings [35,36]. The HVOF technique is suitable for the deposition of both metal and metal–ceramic-based coatings and allows the application of abrasion-resistant coatings [22,37,38]. García-Rodríguez et al. [39] investigated the application of 316L-base HVOF-sprayed coatings on ZE41 magnesium alloy and studied the surface properties. It was found that the application of 316L-based coatings reduced the wear rate (at low wear rates and lower loads) by up to 93% compared to bare ZE41 magnesium alloy. At the same time, the hardness was increased more than six-fold from 65 HV0.1 to 433 HV0.1 by the application of the coatings. Koga et al. [40] reported that the application of amorphous Fe60Cr8Nb8B24 (at.%) HVOF-sprayed coatings can lead to a significant increase in surface hardness, from 222 $\pm$ 5 HV0.3 for steel substrate to 838 $\pm$ 23 HV0.3 for amorphous coating. As reported by the authors [40], the coatings exhibit excellent abrasion properties, mainly due to the higher proportion of the amorphous phase. On the basis of wear measurements, it was observed that the wear rate of the amorphous coatings was approximately two orders of magnitude lower than that of the steel substrate.

With respect to structural defects of HVOF thermally sprayed coatings (pores, microcracks, splat boundaries, etc.), several methods of post-treatment have been studied in the past to improve surface properties. Among them, heat treatment and laser treatment have been used to remove these structural defects [41–43]. Such defects can have a negative effect on both the resulting functional properties and the behavior of the coated samples. The laser remelting process can improve the properties of the coatings by eliminating their defects (pores, cracks, etc.), which can lead to an increase in density, hardness, wear resistance, stress relief, etc.

The aim of this paper was to describe the effect of the laser remelting of Fe-based thermally sprayed coatings deposited on the surface of AZ91 magnesium alloy. Using laser powers of 650 W and 1000 W, the effects of laser remelting on the structure, hardness, and tribological properties of coatings were evaluated. The laser remelting process can be a useful technique for the post-treatment of thermally sprayed coatings and for improving the performance and extending the life of the applied coating or coated part. This issue has not yet received sufficient attention in the literature. The experimental results showed that the application of laser-remelted thermally sprayed Fe-based coatings on AZ91 Mg alloy improves hardness and tribological properties compared to bare Mg alloy and as-sprayed Fe-based coatings.

2. Materials and Methods

2.1. Material

Wrought AZ91 magnesium alloy was used as the substrate for the deposition of thermally sprayed coatings. The elemental composition of AZ91 alloy was (wt%): 8.80 Al; 0.81 Zn; 0.32 Mn; 0.04 Si; 0.01 Zr; balance Mg. The material was received as cast AZ91 magnesium alloy sheets with the dimensions of 100 × 100 × 7 mm. Before the spraying process, the surface of each sheet was corundum blasted with F36 brown corundum (500–600 μm) using a Hunziker ST 1403 (Hunziker, Die Cast Machinery, Waukegan, IL, USA) blasting unit at room temperature under a pressure of 3 bar and then dry air-cleaned.

The surface roughness of the blasted samples (R_a) was determined to be approximately 5.2 μm using a confocal microscope (Lext OLS 3000, Olympus, Tokyo, Japan).

The used feedstock powder (Figure 1) was atomized Fe-based powder for thermal spraying (Diamalloy 1010; Oerlikon Metco, Lomm, The Netherlands) with a nominal size distribution of −45 + 16 μm. The chemical composition of the feedstock powder specified by the supplier was (wt%): 28 Cr; 16 Ni; 4.5 Mo; 1.5 Si; 1.75 C; balance Fe.

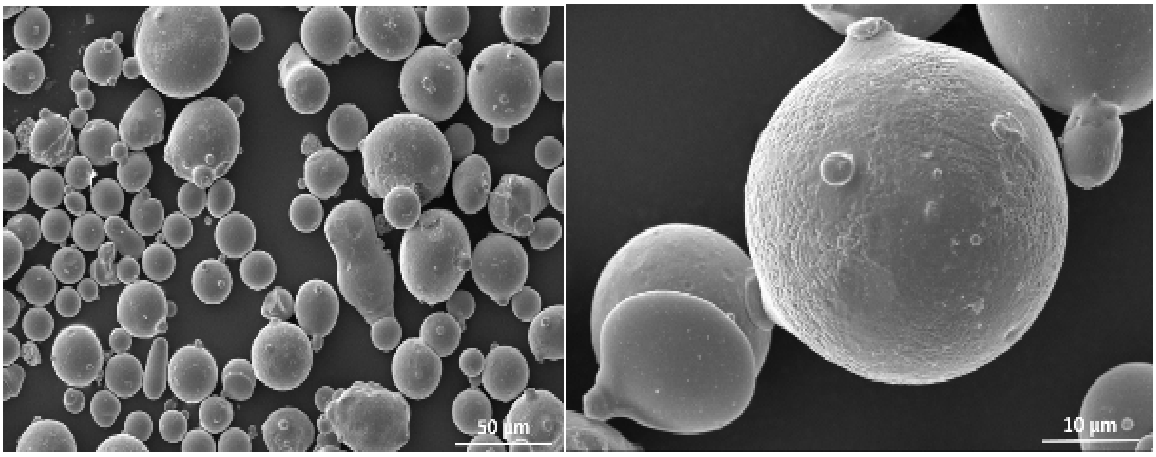

(**a**) (**b**)

Figure 1. The surface morphology of feedstock powder: (**a**) Diamalloy 1010 particles and (**b**) particle detail.

2.2. Thermal Spraying Process

Thermally HVOF-sprayed coatings (sprayed in 4 torch passes) were sprayed on the blasted AZ91 magnesium alloy samples using a JP-5000 liquid-fuel HVOF gun connected to an IRB-2400/16 robot (ABB, Zürich, Switzerland), Figure 2a. The original 100 × 100 mm blasted samples (Figure 2b) were HVOF sprayed along a strip of 100 × 70 mm. The samples were fixed with steel brackets on each side to a distance of 15 mm.

2.3. Laser Treatment Process

Laser treatment was performed on the HVOF-sprayed coatings. The coated magnesium samples were first preheated to 200 °C for 30 min to reduce the heat shock. The laser beam powered by a YLS-2000 fiber laser source (IPG, Oxford, MA, USA) was led by a 100 μm-thick fiber to a Fiber Rhino (Arges, Wackersdorf, Germany) scanning head with an S4LFT1330/328 f-theta lens (Sill Optics, Wendelstein, Germany). The diameter of the beam was 325 μm, and the laser powers were set at 650 W and 1000 W. The linear scanning speed was 4 $m \cdot s^{-1}$ with a line spacing of 60 μm. The laser treatment processing pattern was laid down in the same way as in our previous study [19].

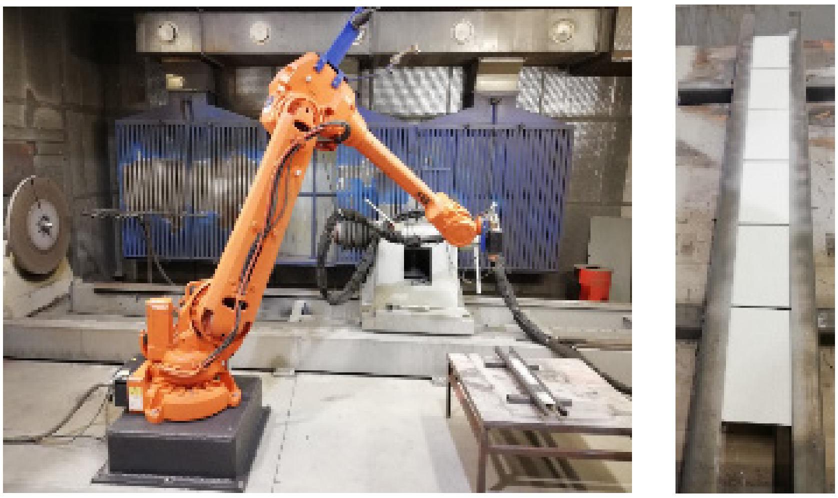

(**a**) (**b**)

Figure 2. Thermal spraying process; (**a**) sample placement for thermal spraying and (**b**) sample holder.

2.4. Characterization

The feedstock powder and the HVOF-sprayed Fe-based coatings were characterized by a JEOL JSM-7600 FESEM microscope equipped with an Ultim® Max energy-dispersive X-ray spectroscope (Oxford Instruments plc, Abingdon, UK). The thicknesses of the different samples were measured from a cross-cut using the SmartSEM® User Interface scanning electron microscope software. Measurements were taken at three locations. EBSD (Electron backscatter diffraction) analysis of the coatings was performed using a JEOL JSM-7600 (JEOL) FESEM microscope equipped with a Nordlys EBSD detector. The accelerating voltage for EBSD analysis was set to 20 kV in order to achieve the best signal:noise ratio and the step size was 0.5 µm. For the EBSD characterization, the samples were ion polished using IB-19500CP Cross Section Polisher (JEOL). The porosity was evaluated by means of image analysis using ImageJ software.

The phase compositions of AZ91 magnesium alloy, feedstock powder, and as-sprayed coatings were determined using an Empyrean X-ray diffraction (XRD) spectrometer (Panalytical, Malvern, UK) with Cu Kα radiation. The 2θ scan range ranged from 10 to 85°; the scan step size was 0.013°; the time per step was set to 39 s; the generator voltage was 40 kV with the tube current 30 mA. HighScore Plus software was used for the evaluation of measured data.

The Vickers microhardness of all samples with thermally sprayed coatings and laser-remelted coatings was measured under an applied load of 300 g for a duration of 10 s (AMH 55, LECO, St. Joseph, MI, USA) according to ASTM E384.

Tribological measurements were performed using the UMT Tribolab (Bruker, Billerica, MA, USA) universal mechanical tester platform using the ball-on-plate method that considers reciprocating motion under an applied normal pin load of 20 N (Mean contact pressure 1150 MPa). The duration was set to 600 s, with a total sliding distance of 12 m at a frequency of 2 Hz, and a working distance (stroke length) of 10 mm. The sliding speed was 20 mm·s^{-1}. The dry sliding wear tests were performed at laboratory temperature on polished samples (Ra $\approx$ 0.05 µm). The counter-ball was Si_3N_4 with a diameter of 7.5 mm. A total of 2 repetitions were performed for each sample.

3. Results and Discussion

3.1. Structural Characterization

Figure 3a–c show the microstructure of HVOF coatings on AZ91 Mg alloy. From the macroscopic point of view, it can be seen that the as-sprayed coating and the coating treated by the 650 W laser power were homogeneous and free of structural defects (Figure 3a,b). For the 1000 W laser remelted coating, extensive cracks were visible, extending to about half of the coating (Figure 3c). As discussed in our previous study [19], the presence of these cracks can be explained by the high stresses in the coating associated with the volume change in the remelted layer. During remelting, pores, splat boundaries and other inhomogeneities in the surface layer disappeared. This led to tensile stresses and crack formation in the coating. There was no visible delamination, deadhesion, or visible oxidation at the coating/Mg substrate interface in any of the coatings, indicating the potentially high adhesion of the coatings to the Mg substrate.

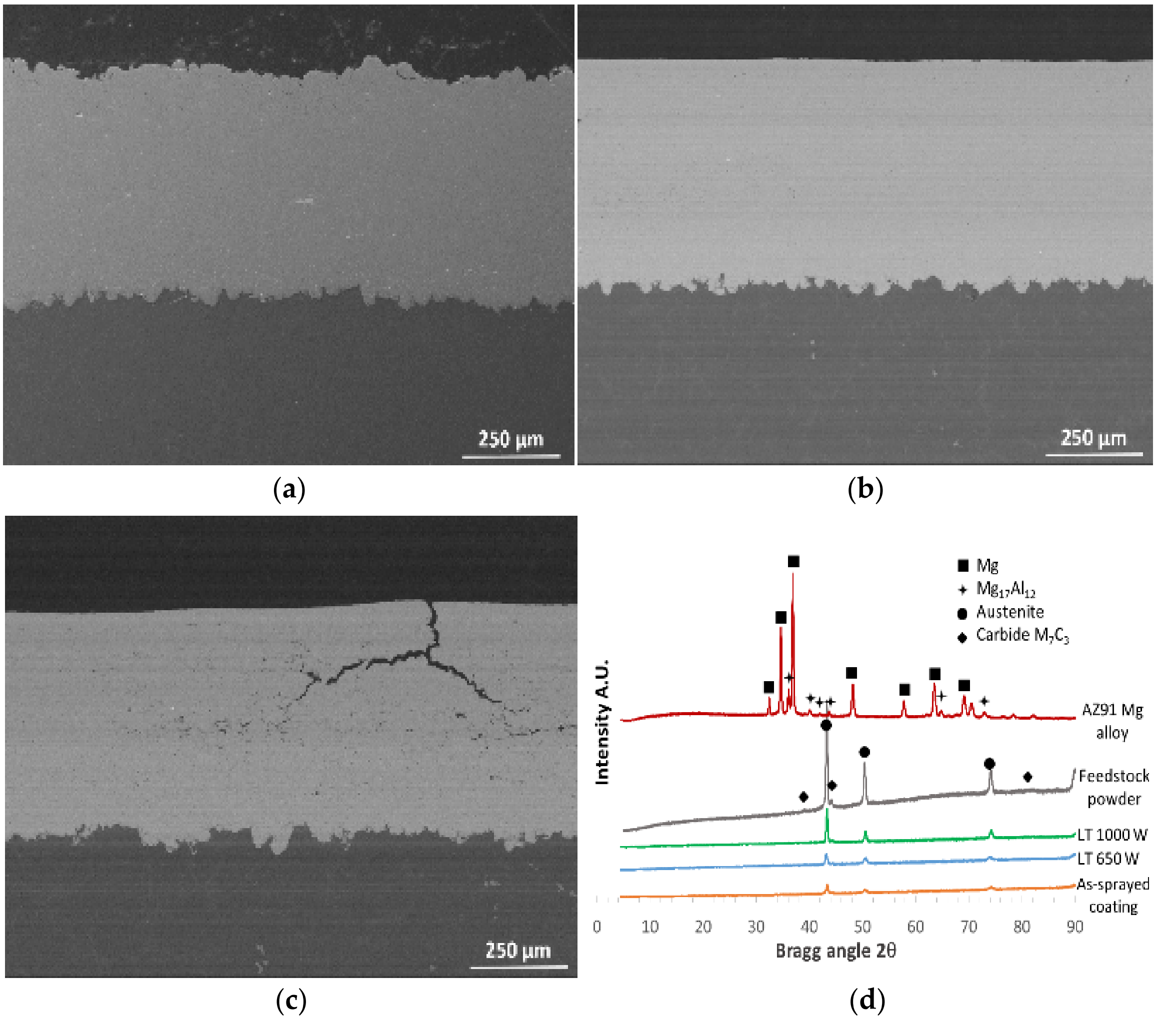

Figure 3. Microstructure of thermally sprayed coatings, (**a**) as-sprayed, (**b**) laser-remelted at 650 W, (**c**) laser-remelted at 1000 W. XRD patterns (**d**) of AZ91 alloy, feedstock powder, and thermally sprayed coatings.

The thicknesses of as-sprayed and laser remelted coatings was about 500 μm. The hardness of the as-sprayed coating was determined to be 535 ± 20 HV0.3. In the case of the remelted coating at a laser power of 650 W, there was an increase in the hardness of the 30 μm-wide remelted layer on the surface to 610 ± 8 HV0.3. In the case of the remelted coating at a laser power of 1000 W, there was an increase in the hardness of the 45 μm wide remelted layer on the surface to 625 ± 5 HV. This increase in hardness may be associated with the disappearance of the splat boundaries, pores, and other microstructural defects. The individual coating thickness values are summarized in Table 1.

Table 1. Microstructural and mechanical features of the coatings and Mg substrate.

Sample	Thickness (μm)	Thickness of Remelted Layer (μm)	Hardness HV0.3	Porosity (%)
AZ91 alloy	-	-	85 ± 9	-
As-sprayed coating	530 ± 25	-	535 ± 20	0.7 ± 0.1
Laser-remelted 650 W	517 ± 10	30 ± 5	610 ± 8	0.0 ± 0.0
Laser-remelted 1000 W	515 ± 9	45 ± 5	625 ± 5	0.0 ± 0.0

The X-ray diffractogram (Figure 3d) of the substrate (AZ91 alloy) showed the presence of two main phases, namely the α-Mg matrix phase (a solid solution of alloying elements in Mg), and the $Mg_{17}Al_{12}$ intermetallic phase. In the case of the feedstock powder, the as-sprayed coating, and the laser-remelted coatings, only two phases were always detected, namely austenite and M_7C_3 carbide, which is a mixed carbide, where M = Fe, Cr, Mo [44,45]. Apart from these peaks, no other phases appeared in the coatings. Compared to the peaks for the feedstock powder, the individual peaks corresponding to the coatings have a lower intensity, which is related to the severe plastic deformation of the particles during the spraying process, and the presence of amorphous areas associated with the impact of fully melted feedstock powder particles on the Mg substrate and their rapid solidification [20,22].

As can be observed in Figure 4, the microstructure of the as-sprayed coating consisted of non-melted, partially melted, and fully melted areas. In Figure 4a, the different regions are clearly distinguishable and include splat boundaries and pores. Figure 4b shows a non-melted particle separated from its surroundings by splat boundaries. As shown by the XRD analysis (Figure 3d), two phases were detected in the coating, and thus in the non-melted area–austenite and M_7C_3 carbide. In the non-melted area, the dendrites of austenite (darker regions) and carbide (lighter regions) were well resolved.

A different microstructure was observed for partially melted areas and significantly deformed areas (Figure 4c). As can be seen in Figure 4c, these areas were composed of fine carbide particles and carbides in the interdendritic space which did not form a continuous network, as in the case of non-melted areas. It appears that during the rapid solidification process, the carbide did not have time to fully crystallize. A high degree of plastic deformation is evident compared to the non-melted region (see Figure 4a).

Fully melted areas were homogeneous. According to the literature [22,40,46], such fully melted areas (Figure 4c) can be assumed to be completely amorphous. These amorphous areas were probably formed as a result of the rapid solidification of the fully melted particle [22,47].

The microstructures of the laser-remelted layers are shown in Figure 5. The thicknesses of the remelted layers at laser powers of 650 W and 1000 W were about 30 μm and 45 μm, respectively. A high-magnification BSE SEM micrograph (Figure 5b,d) shows that the coating was predominantly crystallized after laser remelting. This was also confirmed by the EBSD analysis (see Figure 6a). This was due to the fact that the HVOF coating absorbed a large amount of heat during the remelting process. The microstructure in the laser-remelted layer consisted of columnar grains with a subgrain dendritic microstructure. Individual grains were formed by dendrites of austenite (darker areas) and M_7C_3 carbide (lighter areas) in the interdendritic area (Figure 5b,d). Therefore, remelting did not result in the formation of new phases. This was also confirmed by the XRD analysis above (Figure 3d). As can be seen from the details in Figure 5b,d, the dendritic structure in the remelted layer is similar to the dendritic structure of non-melted particles in the as-sprayed coating (Figure 4b). As can be observed in Figure 5d, in the case of the coating remelted at a laser power of 1000 W, the austenite dendrites and carbides in the remelted layer were coarser than those in the case of the coating remelted at a laser power of 650 W (Figure 5b). This may be due to the fact that more heat was introduced into the coating during remelting with the higher laser power, which resulted in a longer cooling time.

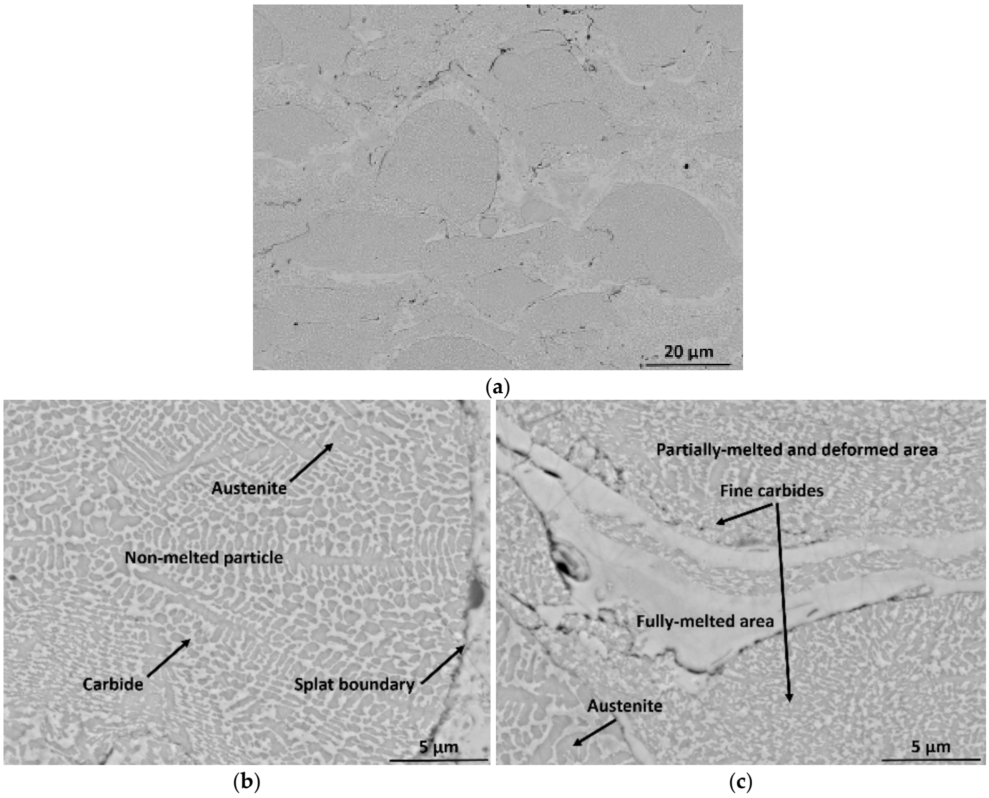

Figure 4. Higher magnification micrograph of as-sprayed coating, (**a**) cross-section, (**b**) detail of non-melted particle, (**c**) detail of melted, deformed and fully melted area.

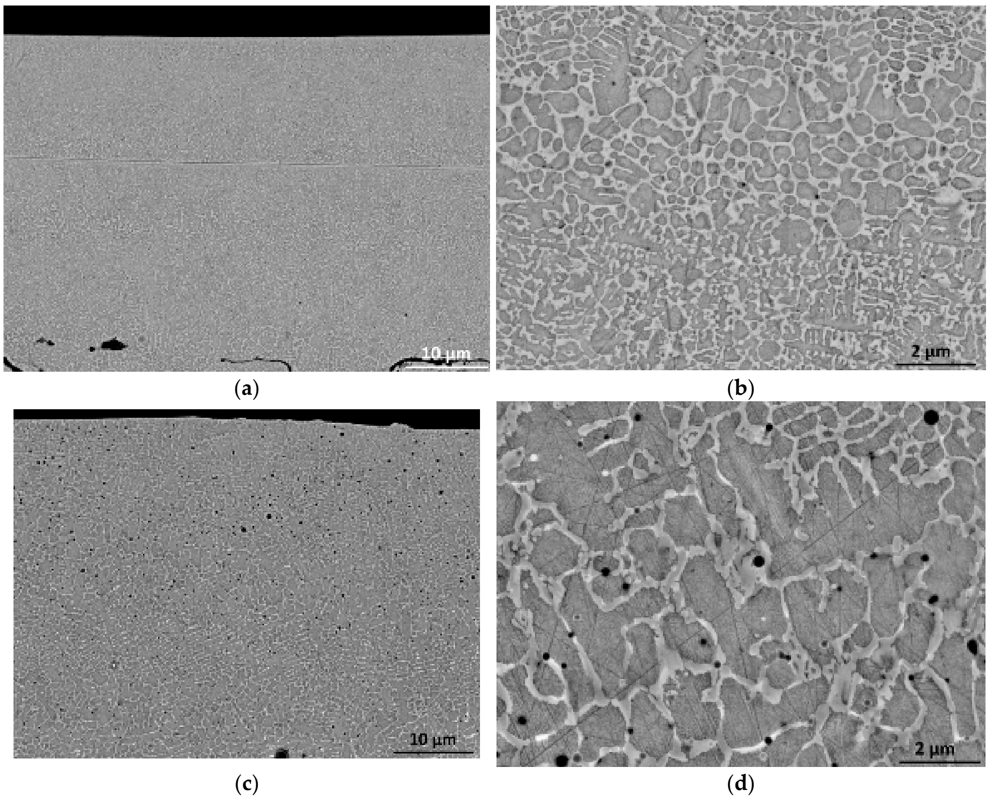

Figure 5. Higher magnification micrograph of laser-remelted coatings, (**a**) coating remelted at 650 W laser power, (**b**) coating remelted at 650 W laser power–detail, (**c**) coating remelted at 1000 W laser power, (**d**) coating remelted at 1000 W laser power–detail.

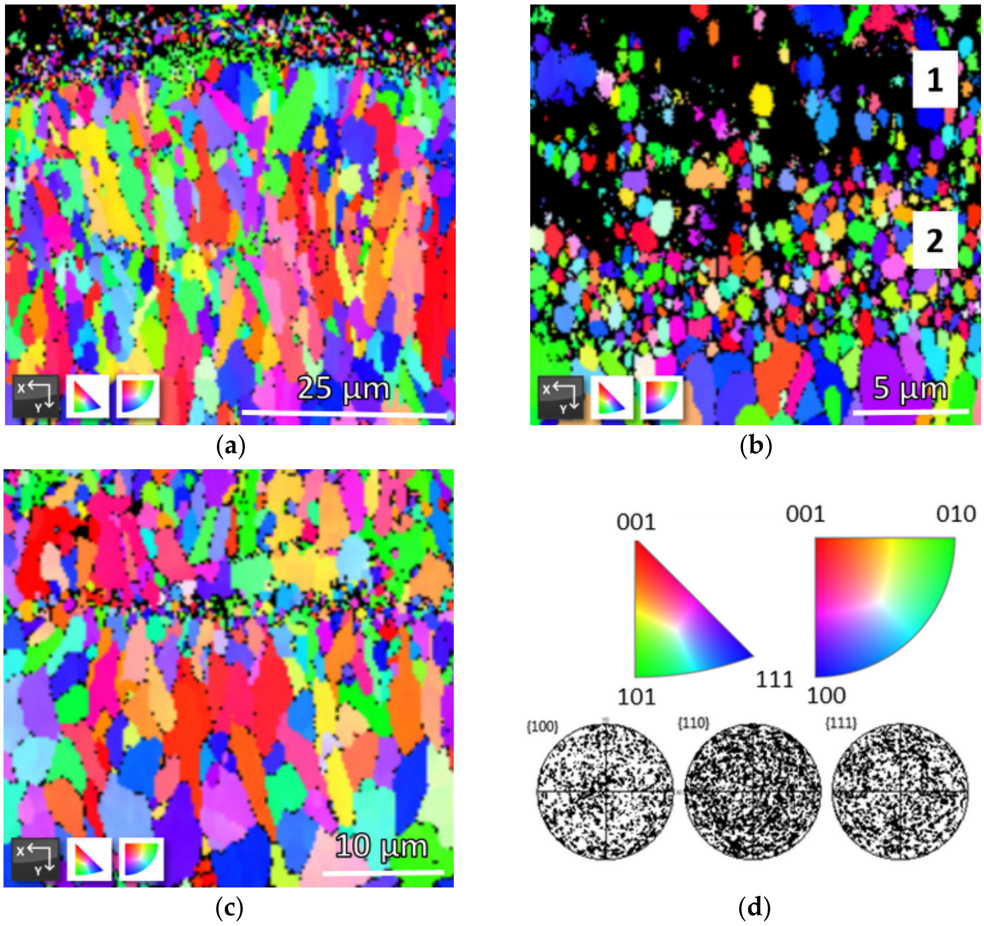

Figure 6. EBSD analysis of LT650W sample, (**a**) overview image of the laser-remelted layer, transition band, and non-affected HVOF coating, (**b**) detail of laser-remelted area, (**c**) detail of (1) non-affected as-sprayed coating and (2) transition band, (**d**) pole figures of the remelted area.

As shown in Figure 6, the as-sprayed coating is predominantly non-crystalline, as very few diffractions were observed. The EBSD results (Figure 6b) suggested that the black areas may be amorphous or pores and splat boundaries, while the non-melted particles and the partially melted and plastically deformed particles retained their crystallinity. Additionally, it may be very fine grains/areas that are smaller than the EBSD characterization step size [48]. There was an approximately 5 µm-thick transition band between the as-sprayed coating and the laser-remelted layer (Figure 6a,c). This was probably the heat-affected zone below the level of the melt pools.

3.2. Tribological Behaviour

Figure 7 summarizes the friction and wear results obtained by the ball-on-plate method performed on AZ91 alloy, the as-sprayed coating surface, and laser-remelted coatings. It can be seen from Figure 7a,b that the lowest value of friction coefficient (COF), 0.24 ± 0.03, was measured for the uncoated AZ91 alloy. In the case of the coated alloy (as-sprayed coating), it was observed that the COF was about 0.45 at the beginning of the testing, but as the sliding distance increased, the COF increased to approx. 0.70. In the case of the laser-remelted coatings at laser powers of 650 and 1000 W, the COF values were comparable—specifically, 0.50 ± 0.05 and 0.48 ± 0.04, respectively. Figure 7a shows that the COF can be considered constant during the measurement. The higher values of the COF for coatings may be due to the higher proportion of carbides in the coating and in the laser-remelted layer. These carbides do not have good sliding properties but increase wear resistance [21,49]. In the case of the as-sprayed coating, the gradual increase in the friction coefficient can be caused by abrasive and tribo-oxidative wear, where deburred and oxidized particles and particles trapped in the open pores of the coating and pits can increase the friction. The COF tends to increase due to the extra energy involved in dragging and pulling debris out of contact between counter-ball and worn surface; thus, the wear tends to increase [50,51].

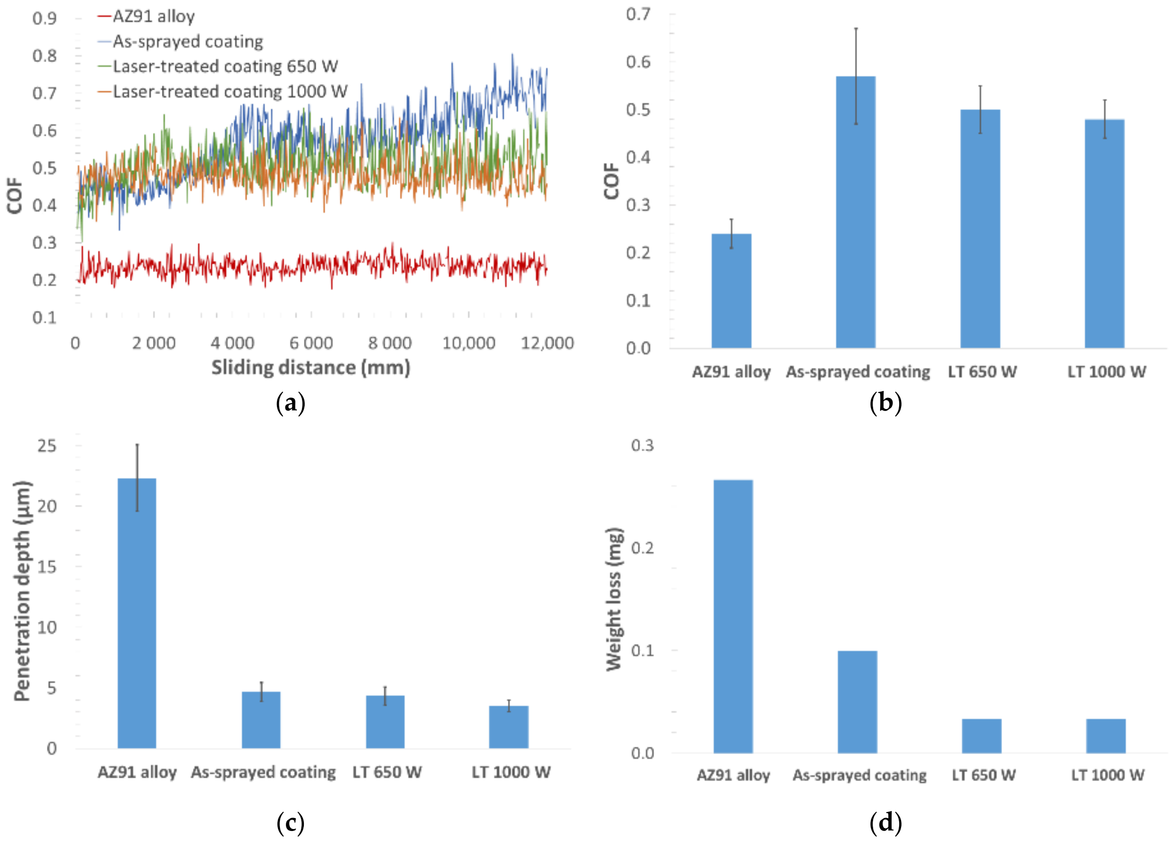

Figure 7. Results of tribological testing for individual samples: (**a**) record of the friction coefficients (COF), (**b**) COF values, (**c**) penetration depth values, (**d**) weight loss values. In the case of Figure (**d**), the error bars are not shown because the measurement error (weight change) was close to zero.

Even though the lowest COF value was obtained for the uncoated AZ91 alloy, the wear rate, penetration depth, and weight loss were significantly higher than for the coated samples (Figure 7c,d). The penetration depth after the wear test was approximately 4–5 times lower for the coated samples than for the uncoated AZ91 alloy.

The weight loss was also significantly lower for the coated samples. In the case of AZ91 alloy, the weight loss was determined to be 2.7×10^{-4} g, while in the case of the as-sprayed coating, the weight loss was 1×10^{-4} g. In the case of laser-remelted coatings, the weight loss was even lower, at 3.3×10^{-5} g.

Wear tracks and wear profiles of the tested samples are shown in Figure 8. The individual dimensions of the wear tracks correlate with the weight loss results. As shown in Figure 8a, in the case of alloy AZ91, the penetration depth of the wear track at the lowest point was about 30 μm. The width of the wear track was approximately 1200 μm after the wear test. The spraying of the coating increased the wear resistance of samples and thus decreased the penetration depth. The penetration depth was determined to be 5 μm in the case of the as-sprayed coating, and the wear trace width was determined to be 650 μm (Figure 8b). The remelting of the thermally sprayed (as-sprayed) coating at a laser power of 650 or 1000 W led to a further increase in wear resistance. The penetration depth after the wear test of the remelted coatings was determined to be approximately 4 μm in both cases, and the width of the wear tracks was approximately 430 μm (Figure 8c,d).

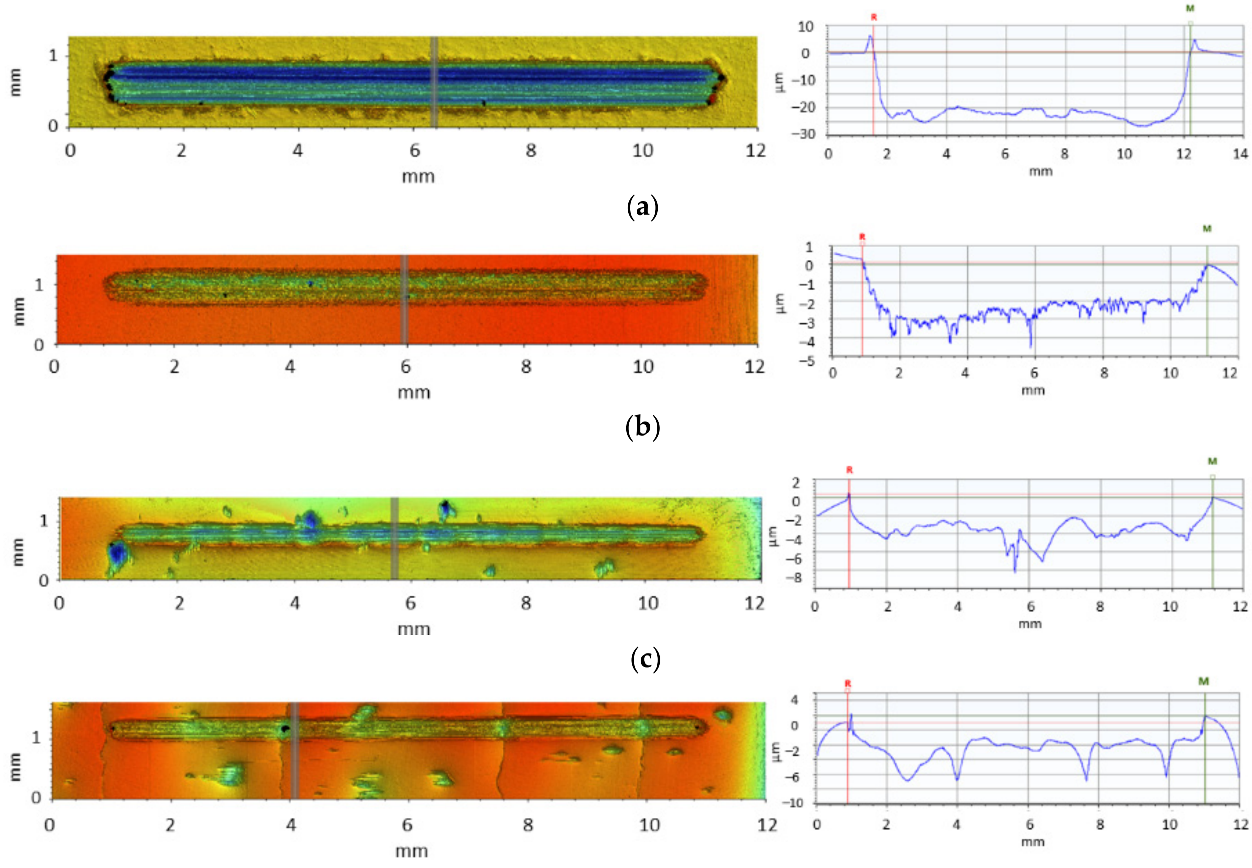

Figure 8. Wear tracks and wear profiles of tested samples, (**a**) AZ91 magnesium alloy, (**b**) as-sprayed coating, (**c**) laser-treated coating (650 W), (**d**) laser-treated coating (1000 W).

The wear track of AZ91 magnesium alloy is shown in Figure 9a,b. From a macroscopic point of view, grooves (abrasive wear) were evident in the wear direction (Figure 9a). Upon closer examination (Figure 9b), it was evident that the Mg alloy surface was showing cracks, as well as delamination (flaking) of the Mg alloy, and there were also obvious areas of oxidation after the wear. The oxidation of the surface was also recorded via EDS analysis (Figure 10a).

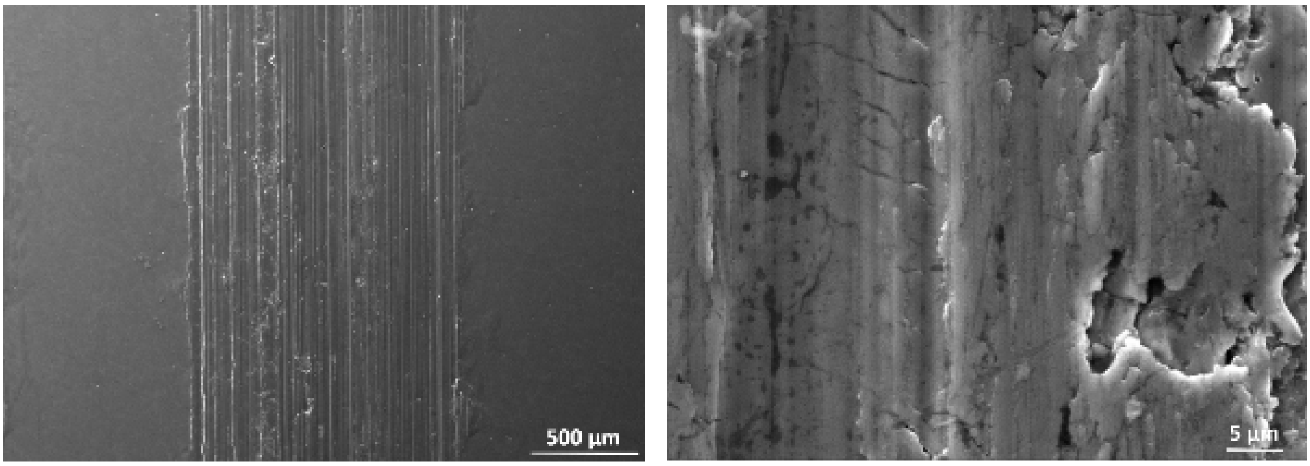

(**a**) (**b**)

Figure 9. *Cont.*

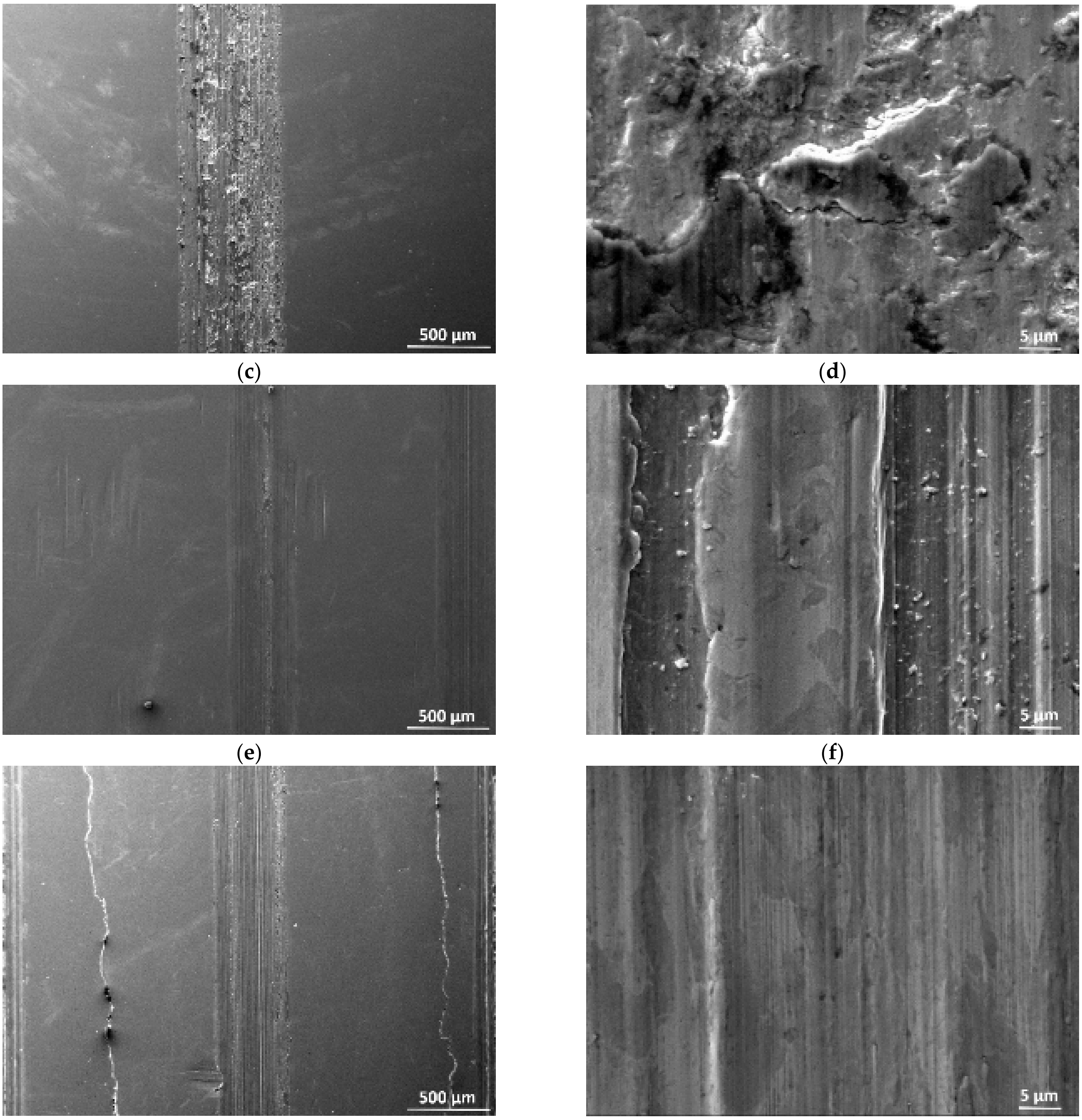

Figure 9. Wear track of (**a**) AZ91 magnesium alloy, (**b**) AZ91 magnesium alloy detail, (**c**) as-sprayed coating, (**d**) as-sprayed coating detail, (**e**) laser-treated coating (650 W), (**f**) laser-treated coating (650 W) detail, (**g**) laser-treated coating (1000 W), (**h**) laser-treated coating (1000 W) detail.

Feng [52] and other authors [53,54] report that during friction and wear tests, intermetallic phases are, in the case of AZ-based Mg alloys, a ready source of cracks at the solid solution α-Mg/intermetallic phase interface due to the fact that the intermetallic phases (especially β-$Mg_{17}(Al,Zn)_{12}$ and Al_8Mn_5 phases) are more brittle than the surrounding matrix α-Mg. In addition, for AZ91 alloy, the β-$Mg_{17}(Al,Zn)_{12}$ phase loses adhesion to the surrounding α-Mg matrix during plastic deformation. This can adversely affect the mechanical properties of the alloy. Previous studies [54,55] have shown that due to the heat treatment, the β-$Mg_{17}(Al,Zn)_{12}$ phase can be dissolved in the surrounding matrix, thereby significantly improving the wear resistance.

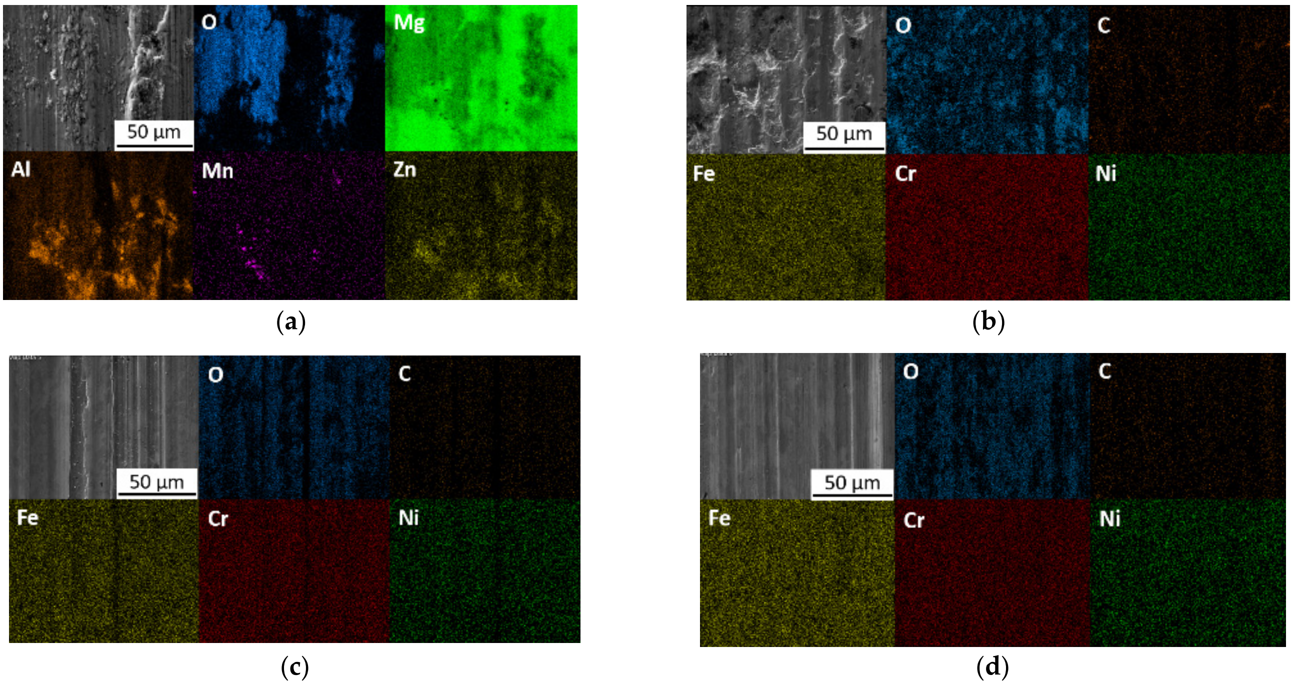

Figure 10. EDS mapping of worn surfaces, (**a**) AZ91 magnesium alloy, (**b**) as-sprayed coating, (**c**) laser-treated coating (650 W), (**d**) laser-treated coating (1000 W).

The main reasons for wear in Mg alloy are abrasion, crack formation, and subsequent delamination. In accordance with the literature [52,54,56,57], the wear mechanism consists of the initiation of a crack at the α-Mg/intermetallic phase interface, which further propagates through the substrate to the surface. This leads to the formation of macrocracks and surface metal delamination, which subsequently forms pits in the surface, increasing the surface roughness, as documented in Figure 9a,b. A large amount of frictional heat is generated at the counter-ball/sample interface during wear and friction. Studies [1,57,58] have shown that the β-$Mg_{17}(Al,Zn)_{12}$ phase does not have a significant hardening effect at grain boundaries during dry friction. In addition, the β-$Mg_{17}(Al,Zn)_{12}$ phase can delaminate during friction and can even be completely pulled into the space between the surface and the counter-ball, causing abrasive effects [53]. Chen [53] states that as the sliding speed of the counter-ball increases, the frictional heat increases and thus the plasticity of the Mg alloy increases; therefore, not as many cracks form in the material.

However, due to friction in the air (depending on the speed and load), a thin layer of magnesium oxide forms on the surface of the Mg substrate, leading to significant oxidative wear of the surface (Figure 10a). Upon friction, the MgO layer breaks down, peels off, erodes, and exposes a new surface that can oxidize further. The detached MgO residues can continue to abrade the surface (tribo-oxidative wear). This phenomenon is continuously repeated and the oxidative wear increases.

In the case of the as-sprayed coating, mainly abrasive and tribo-oxidative wear was observed (Figure 9c,d). Closed pores and splat boundaries were exposed. Abraded particles, debris, and oxides (formed during the friction) were able to fill the exposed pores in the coating (Figure 9d). Upon close inspection (Figure 9d), crack formation and delamination were observed in the case of as-sprayed coatings due to the depletion of the plasticity of the austenite matrix. In addition, the coating showed tribo-oxidative wear (Figure 10b).

Regarding the wear mechanism, on the basis of available sources [59,60], it was found that at the carbide/matrix phase interface or at splat or pore boundaries, a crack initiates due to friction, which subsequently propagates through the surface layer of the material. This then leads to the formation of macrocracks in plastically deformed regions due to local plasticity depletion [61]. Subsequently, with further wear, delamination of the surface occurs [39]. Bolelli [21] mentioned that fatigue failure of the material occurs during the cyclic loading of coatings. The resulting pits and grooves, etc., on the surface of the coating are the result of fatigue cracks that initiate and propagate along splat boundaries and non-melted particles. At the same time, the surface of the wear track may be covered by a discontinuous layer of abraded particles and oxides formed during the release of frictional heat. The presence of these deburred and oxidized particles was also observed on the surface of the coatings (Figures 9c and 10b). The deburred and oxidized particles and debris on the surface could lead to an increase in the COF, as shown in Figure 7a.

In the case of laser-remelted coatings at a laser power of 650 W (Figure 9e,f) or 1000 W (Figure 9g,h), only abrasive wear and tribo-oxidative wear were observed, where oxidation of the surface of the worn coating occurred due to the frictional heat released (Figure 10c,d). No cracking or delamination occurred due to the compact structure and high carbide content. Tabrett [62] and other authors [45,63,64] reported that the carbides present in the coating structure can provide wear protection due to their hardness. The austenitic matrix has good ductility and plasticity. The role of the matrix is to provide mechanical support to the carbides, and in turn the carbides protect the matrix from wear. If there are few carbides in the coating structure, the matrix is not sufficiently protected against wear and is preferentially deformed and removed during the wear. Wear resistance is expected to increase with an increasing volume of carbides in the coating structure [21,44,62].

4. Conclusions

- Fe-based coatings were thermally sprayed on the surface of AZ91 magnesium alloy via the HVOF method using commercially available powders.
- Laser remelting of the coating surface layer resulted in a change in the microstructure in the 30 ± 5 µm or 45 ± 5 µm-thick remelted layer.
- Laser remelting of the thermally sprayed coating resulted in the disappearance of porosity and an increase in the hardness of the coating up to 625 ± 5 HV0.3.
- The remelting of the coating at 1000 W laser power resulted in cracks in the coating due to internal stresses and volume changes.
- On the basis of tribological measurements performed by the ball-on-plate method, it was shown that the sprayed coatings and laser-remelted coatings had a higher value of COF than the uncoated AZ91 alloy; however, surface-treated samples showed significantly lower wear rates and lower weight loss values (five times lower).

Author Contributions: M.B. (Martin Buchtík) and L.D. conceived and designed the experiments and methodology and wrote the paper, M.B. (Martin Buchtík) performed experiments (metallography); M.B. (Matěj Březina) and J.W. performed experiments, measurements and analyzed data (SEM + EDS); J.F. (Jan Filipenský) and M.P. performed the deposition of coatings and performed experiments. L.M. and P.D. performed experiments (laser remelting) and performed evaluation. D.N. and J.F. (Josef Frýza) performed tribological measurements and analyzed and evaluated data. D.K. performed experiments (EBSD analysis). All authors have read and agreed to the published version of the manuscript.

Funding: This work was supported by Specific University Research at FCH BUT, Project No. FCH-S-23-8208, Ministry of Education, Youth and Sports of the Czech Republic. The research was also financially supported by the Science Grant Agency of the Slovak Republic through project No. 1/0153/21.

Institutional Review Board Statement: Not applicable.

Informed Consent Statement: Not applicable.

Data Availability Statement: The data supporting the results are included in the article.

Conflicts of Interest: The authors declare no conflict of interest.

References

1. Friedrich, H.E.; Mordike, B.L. *Magnesium Technology: Metallurgy, Design Data, Applications*; Springer: Berlin/Heidelberg, Germany, 2006; pp. 1–677.
2. Braszczyńska-Malik, K.N. Discontinuous and continuous precipitation in magnesium–aluminium type alloys. *J. Alloys Compd.* **2009**, *477*, 870–876. [CrossRef]
3. Parco, M.; Zhao, L.; Zwick, J.; Bobzin, K.; Lugscheider, E. Investigation of HVOF spraying on magnesium alloys. *Surf. Coat. Technol.* **2006**, *201*, 3269–3274. [CrossRef]
4. Kulekci, M.K. Magnesium and its alloys applications in automotive industry. *Int. J. Adv. Manuf. Technol.* **2008**, *39*, 851–865. [CrossRef]
5. Mordike, B.L.; Ebert, T. Magnesium: Properties—Applications—Potential. *Mater. Sci. Eng. A* **2001**, *302*, 37–45. [CrossRef]
6. Hu, L.; Meng, Q.; Chen, S.; Wang, H. Effect of Zn content on the chemical conversion treatments of AZ91D magnesium alloy. *Appl. Surf. Sci.* **2012**, *259*, 816–823. [CrossRef]
7. Pekguleryuz, M. Magnesium casting alloys. *Magn. Technol. Metall. Des. Data Appl.* **2006**, 145–218. [CrossRef]
8. Song, G.L. Corrosion and Protection of Magnesium Alloys: An Overview of Research Undertaken by CAST. *Mater. Sci. Forum* **2005**, *488–489*, 649–652. [CrossRef]
9. Song, G.-L. *Corrosion Prevention of Magnesium Alloys*; Woodhead Publishing: Sawston, UK, 2013; 562p.
10. Song, G.-L. *Corrosion of Magnesium Alloys*; Woodhead Publishing: Sawston, UK, 2011; 640p.
11. Zhao, M.C.; Liu, M.; Song, G.L.; Atrens, A. Influence of Homogenization Annealing of AZ91 on Mechanical Properties and Corrosion Behavior. *Adv. Eng. Mater.* **2008**, *10*, 93–103. [CrossRef]
12. Iwaszko, J.; Strzelecka, M. Microstructure and Corrosion Resistance of AZ91 Magnesium Alloy after Surface Remelting Treatment. *Materials* **2022**, *15*, 8980. [CrossRef] [PubMed]
13. Hadzima, B.; Kajánek, D.; Jambor, M.; Drábiková, J.; Březina, M.; Buhagiar, J.; Pastorková, J.; Jacková, M. PEO of AZ31 Mg Alloy: Effect of Electrolyte Phosphate Content and Current Density. *Metals* **2020**, *10*, 1521. [CrossRef]
14. Shulha, T.; Serdechnova, M.; Lamaka, S.V.; Lu, X.; Feiler, C.; Blawert, C.; Zheludkevich, M.L. Corrosion Inhibitors Intercalated into Layered Double Hydroxides Prepared In Situ on AZ91 Magnesium Alloys: Structure and Protection Ability. *ACS Appl. Mater. Interfaces* **2023**, *15*, 6112. [CrossRef]
15. Doskočil, L.; Šomanová, P.; Másilko, J.; Buchtík, M.; Hasoňová, M.; Kalina, L.; Wasserbauer, J. Characterization of Prepared Superhydrophobic Surfaces on AZ31 and AZ91 Alloys Etched with ZnCl2 and SnCl2. *Coatings* **2022**, *12*, 1414. [CrossRef]
16. Buchtík, M.; Kosár, P.; Wasserbauer, J.; Tkacz, J.; Doležal, P. Characterization of Electroless Ni–P Coating Prepared on a Wrought ZE10 Magnesium Alloy. *Coatings* **2018**, *8*, 96. [CrossRef]
17. Buchtík, M.; Krystỳnová, M.; Másilko, J.; Wasserbauer, J. The Effect of Heat Treatment on Properties of Ni–P Coatings Deposited on a AZ91 Magnesium Alloy. *Coatings* **2019**, *9*, 461. [CrossRef]
18. Wasserbauer, J.; Buchtík, M.; Brescher, R. Investigation of Ni-P coatings on AZ91 cast magnesium alloy. In Proceedings of the 28th International Conference on Metallurgy and Materials, Brno, Czech Republic, 22–24 May 2019; pp. 1192–1196.
19. Buchtík, M.; Hasoňová, M.; Horník, P.; Březina, M.; Doskočil, L.; Másilko, J.; Mrňa, L.; Filipenský, J.; Kuběna, I.; Fintová, S.; et al. Influence of laser remelting on the microstructure and corrosion behavior of HVOF-sprayed Fe-based coatings on magnesium alloy. *Mater. Charact.* **2022**, *194*, 112343. [CrossRef]
20. Milanti, A.; Matikainen, V.; Bolelli, G.; Koivuluoto, H.; Lusvarghi, L.; Vuoristo, P. Microstructure and Sliding Wear Behavior of Fe-Based Coatings Manufactured with HVOF and HVAF Thermal Spray Processes. *J. Therm. Spray Technol.* **2016**, *25*, 1040–1055. [CrossRef]
21. Bolelli, G.; Berger, L.M.; Börner, T.; Koivuluoto, H.; Lusvarghi, L.; Lyphout, C.; Markocsan, N.; Matikainen, V.; Nylén, P.; Sassatelli, P.; et al. Tribology of HVOF- and HVAF-sprayed WC–10Co4Cr hardmetal coatings: A comparative assessment. *Surf. Coat. Technol.* **2015**, *265*, 125–144. [CrossRef]
22. Fauchais, P.L.; Heberlein, J.V.R.; Boulos, M.I. *Thermal Spray Fundamentals: From Powder to Part*; Springer Science & Business Media: Berlin/Heidelberg, Germany, 2014; pp. 1–1566.
23. Sobolev, V.V.; Guilemany, J.M.; Nutting, J.; Joshi, S. *High Velocity Oxy-Fuel Spraying: Theory, Structure-Property Relationships and Applications*; Maney: London, UK, 2004; p. 397.
24. Liu, C.; Zheng, H.; Gu, X.; Jiang, B.; Liang, J. Effect of severe shot peening on corrosion behavior of AZ31 and AZ91 magnesium alloys. *J. Alloys Compd.* **2019**, *770*, 500–506. [CrossRef]
25. Bagherifard, S.; Hickey, D.J.; Fintová, S.; Pastorek, F.; Fernandez-Pariente, I.; Bandini, M.; Webster, T.J.; Guagliano, M. Effects of nanofeatures induced by severe shot peening (SSP) on mechanical, corrosion and cytocompatibility properties of magnesium alloy AZ31. *Acta Biomater.* **2018**, *66*, 93–108. [CrossRef] [PubMed]
26. Wagner, L. *Shot Peening*; Wiley-VCH Verlag GmbH & Co. KGaA: Weinheim, Germany, 2003.
27. Guo, Y.; Wang, S.; Liu, W.; Sun, Z.; Zhu, G.; Xiao, T. Effect of laser shock peening on tribological properties of magnesium alloy ZK60. *Tribol. Int.* **2020**, *144*, 106138. [CrossRef]
28. Jiang, J.; Hou, W.; Feng, X.; Shen, Y. Oxidation resistant FeCoNiCrAl high entropy alloy/AlSi12 composite coatings with excellent adhesion on Ti-6Al-4 V alloy substrate via mechanical alloying and subsequent laser cladding. *Surf. Coat. Technol.* **2023**, *464*, 129577. [CrossRef]

29. Hou, W.; Ding, Y.; Huang, G.; Huda, N.; Shah, L.H.A.; Piao, Z.; Shen, Y.; Shen, Z.; Gerlich, A. The role of pin eccentricity in friction stir welding of Al-Mg-Si alloy sheets: Microstructural evolution and mechanical properties. *Int. J. Adv. Manuf. Technol.* **2022**, *121*, 7661–7675. [CrossRef]
30. Song, Y.L.; Yao, A.E.; Liu, H.; Yu, A.S.R.; Zhu, A.X.Y.; Wang, A.S.H. Effect of neodymium on microstructure and corrosion resistance of AZ91 magnesium alloy. *J. Mater. Sci.* **2007**, *42*, 4435–4440. [CrossRef]
31. Ling, W. Effect of Neodymium on Microstructure and Mechanical Properties of Mg-Sb Alloy. *J. Rare Earths* **2006**, *24*, 376–378. [CrossRef]
32. Lin, H.; Yang, M.; Tang, H.; Pan, F. Effect of minor Sc on the microstructure and mechanical properties of AZ91 Magnesium Alloy. *Prog. Nat. Sci. Mater. Int.* **2018**, *28*, 66–73. [CrossRef]
33. Bonnah, R.C.; Fu, Y.; Hao, H. Microstructure and mechanical properties of AZ91 magnesium alloy with minor additions of Sm, Si and Ca elements. *China Foundry* **2019**, *16*, 319–325. [CrossRef]
34. Liu, Y.Z.; Hu, X.B.; Zheng, S.J.; Zhu, Y.L.; Wei, H.; Ma, X.L. Microstructural evolution of the interface between NiCrAlY coating and superalloy during isothermal oxidation. *J. Mater.* **2015**, *80*, 63–69. [CrossRef]
35. Deforce, B.S.; Eden, T.J.; Potter, J.K. Cold spray Al-5% Mg coatings for the corrosion protection of magnesium alloys. *J. Therm. Spray Technol.* **2011**, *20*, 1352–1358. [CrossRef]
36. Yao, H.L.; Yi, Z.H.; Yao, C.; Zhang, M.X.; Wang, H.T.; Li, S.B.; Bai, X.B.; Chen, Q.Y.; Ji, G.C. Improved corrosion resistance of AZ91D magnesium alloy coated by novel cold-sprayed Zn-HA/Zn double-layer coatings. *Ceram. Int.* **2019**, *46*, 7687–7693. [CrossRef]
37. Röttger, A.; Weber, S.; Theisen, W.; Rajasekeran, B.; Vassen, R. Mechanical properties of thermally sprayed Fe based coatings. *Mater. Sci. Technol.* **2011**, *27*, 973–982. [CrossRef]
38. Guo, S.F.; Pan, F.S.; Zhang, H.J.; Zhang, D.F.; Wang, J.F.; Miao, J.; Su, C.; Zhang, C. Fe-based amorphous coating for corrosion protection of magnesium alloy. *Mater. Des.* **2016**, *108*, 624–631. [CrossRef]
39. García-Rodríguez, S.; Torres, B.; Lopez, A.J.; Rainforth, W.M.; Otero, E.; Muñoz, M.; Rams, J. Wear Resistance of Stainless Steel Coatings on ZE41 Magnesium Alloy. *J. Therm. Spray Technol.* **2018**, *27*, 1615–1631. [CrossRef]
40. Koga, G.Y.; Schulz, R.; Savoie, S.; Nascimento, A.R.C.; Drolet, Y.; Bolfarini, C.; Kiminami, C.S.; Botta, W.J. Microstructure and wear behavior of Fe-based amorphous HVOF coatings produced from commercial precursors. *Surf. Coat. Technol.* **2017**, *309*, 938–944. [CrossRef]
41. Verdian, M.M. 3.13 Finishing and Post-Treatment of Thermal Spray Coatings. *Compr. Mater. Finish.* **2017**, *3*, 191–206.
42. Das, B.; Gopinath, M.; Nath, A.K.; Bandyopadhyay, P.P. Effect of cooling rate on residual stress and mechanical properties of laser remelted ceramic coating. *J. Eur. Ceram. Soc.* **2018**, *38*, 3932–3944. [CrossRef]
43. Fu, B.Y.; He, D.Y.; Zhao, L.D. Effect of heat treatment on the microstructure and mechanical properties of Fe-based amorphous coatings. *J. Alloys Compd.* **2009**, *480*, 422–427. [CrossRef]
44. Wieczerzak, K.; Bala, P.; Stepien, M.; Cios, G.; Koziel, T. Formation of eutectic carbides in Fe–Cr–Mo–C alloy during non-equilibrium crystallization. *Mater. Des.* **2016**, *94*, 61–68. [CrossRef]
45. Wieczerzak, K.; Bala, P.; Dziurka, R.; Tokarski, T.; Cios, G.; Koziel, T.; Gondek, L. The effect of temperature on the evolution of eutectic carbides and M7C3→M23C6 carbides reaction in the rapidly solidified Fe-Cr-C alloy. *J. Alloys Compd.* **2017**, *698*, 673–684. [CrossRef]
46. Koga, G.Y.; Wolf, W.; Schulz, R.; Savoie, S.; Bolfarini, C.; Kiminami, C.S.; Botta, W.J. Corrosion and wear properties of FeCrMnCoSi HVOF coatings. *Surf. Coat. Technol.* **2019**, *357*, 993–1003. [CrossRef]
47. Ashby, M.F.; Greer, A.L. Metallic glasses as structural materials. *Scr. Mater.* **2006**, *54*, 321–326. [CrossRef]
48. Samal, S.; Tyc, O.; Cizek, J.; Klecka, J.; Lukáč, F.; Molnárová, O.; de Prado, E.; Weiss, Z.; Kopeček, J.; Heller, L.; et al. Fabrication of thermal plasma sprayed niti coatings possessing functional properties. *Coatings* **2021**, *11*, 610. [CrossRef]
49. de Oliveira, M.M.; Costa, H.L.; Silva, W.M.; de Mello, J.D.B. Effect of iron oxide debris on the reciprocating sliding wear of tool steels. *Wear* **2019**, *426–427*, 1065–1075. [CrossRef]
50. Yuan, C.Q.; Peng, Z.; Zhou, X.C.; Yan, X.P. The characterization of wear transitions in sliding wear process contaminated with silica and iron powder. *Tribol. Int.* **2005**, *38*, 129–143. [CrossRef]
51. Santanam, N. Effect of wear debris on wear in rolling-sliding motion. *Wear* **1983**, *90*, 261–267. [CrossRef]
52. Feng, A.H.; Ma, Z.Y. Enhanced mechanical properties of Mg–Al–Zn cast alloy via friction stir processing. *Scr. Mater.* **2007**, *56*, 397–400. [CrossRef]
53. Chen, Q.; Zhao, Z.; Zhu, Q.; Wang, G.; Tao, K. Cerium addition improved the dry slidingwear resistance of surface welding AZ91 alloy. *Materials* **2018**, *11*, 250. [CrossRef]
54. Lit, Y.Z.; Wang, Q.D.; Ding, W.J.; Zeng, X.Q.; Zhu, Y.P. Fracture behavior of AZ91 magnesium alloy. *Mater. Lett.* **2000**, *44*, 265–268.
55. Chen, Q.; Li, K.; Liu, Y.; Zhao, Z.; Tao, K.; Zhu, Q. Effects of heat treatment on the wear behavior of surfacing AZ91 magnesium alloy. *J. Mater. Res.* **2017**, *32*, 2161–2168. [CrossRef]
56. Xia, S.; Liu, Y.; Fu, D.; Jin, B.; Lu, J. Effect of Surface Mechanical Attrition Treatment on Tribological Behavior of the AZ31 Alloy. *J. Mater. Sci. Technol.* **2016**, *32*, 1245–1252. [CrossRef]
57. Zafari, A.; Ghasemi, H.M.; Mahmudi, R. An investigation on the tribological behavior of AZ91 and AZ91+3wt% RE magnesium alloys at elevated temperatures. *Mater. Des.* **2014**, *54*, 544–552. [CrossRef]

58. Braszczyńska-Malik, K.N. Spherical shape of γ-Mg17Al12 precipitates in AZ91 magnesium alloy processed by equal-channel angular pressing. *J. Alloys Compd.* **2009**, *487*, 263–268. [CrossRef]
59. Myshkin, N.K.; Grigoriev, A.Y. Scale factor in tribology: Roughness and texture. In *2015 IFToMM World Congress Proceedings, IFToMM 2015*; National Taiwan University: Taiwan, 2015.
60. Rivera-Tello, C.D.; Broitman, E.; Flores-Ruiz, F.J.; Perez-Alvarez, J.; Flores-Jiménez, M.; Jiménez, O.; Flores, M. Micro and macro-tribology behavior of a hierarchical architecture of a multilayer tan/ta hard coating. *Coatings* **2020**, *10*, 263. [CrossRef]
61. Kasama, A.H.; Cava, R.D.; Mourisco, A.; Kiminami, C.S.; Bolfarini, C. Microstructure of spray formed 2.9%C-22%Cr high chromium white cast iron. *Mater. Sci. Forum* **2003**, *416–418*, 419–424. [CrossRef]
62. Tabrett, C.P.; Sare, I.R.; Ghomashchi, M.R. Microstructure-property relationships in high chromium white iron alloys. *Int. Mater. Rev.* **1996**, *41*, 59–82. [CrossRef]
63. Wang, K.; Chang, B.; Lei, Y.; Fu, H.; Lin, Y. Effect of cobalt on microstructure and wear resistance of Ni-based alloy coating fabricated by laser cladding. *Metals* **2017**, *7*, 551. [CrossRef]
64. Zhang, D.; Yu, R.; Chen, K.; Yang, X.; Liu, Y.; Yin, Y. Corrosion and corrosion-friction properties of plasma cladding wear-resistant layer on Fe-based alloy. *Mater. Res. Express* **2018**, *5*, 026525. [CrossRef]